Photoluminescence of $KZnF_3:Tl^+$ and $KMgF_3:Tl^+$ crystals

2002 J. Phys.: Condens. Matter 14 13835

(http://iopscience.iop.org/0953-8984/14/50/310)

INSTITUTE OF PHYSICS PUBLISHING JOURNAL OF PHYSICS: CONDENSED MATTER

J. Phys.: Condens. Matter **14** (2002) 13835–13856 PII: S0953-8984(02)52917-9

Photoluminescence of $KZnF_3$:Tl^+ and $KMgF_3$:Tl^+ crystals

L K Aminov, S I Nikitin, N I Silkin[1], A A Shakhov and R V Yusupov

Kazan State University, Kremlevskaya 18, 420008 Kazan, Russia

E-mail: Nikolai.Silkin@ksu.ru

Received 2 September 2002
Published 6 December 2002
Online at stacks.iop.org/JPhysCM/14/13835

Abstract

The luminescence spectra of $KZnF_3$:Tl^+ and $KMgF_3$:Tl^+ crystals with a perovskite structure were investigated in the temperature range of 4.2–300 K and at optical excitation in the A absorption band (∼6 eV). The spectrum of $KZnF_3$:Tl^+ at 300 K is a wide band with the maximum E_{max} at 5.48 eV and the width of about 0.47 eV. At 100 K the band splits into two components: an intensive one with $E_{max} = 5.63$ eV and a width of about 0.2 eV and a weak one with $E_{max} = 4.66$ eV. At 4.2 K an intensive broad band practically disappears and a narrow line accompanied by a vibration structure is observed at $E = 5.725$ eV. This line is assigned to a zero-phonon transition from the metastable $^3\Gamma_{1u}$ level to the ground $^1\Gamma_{1g}$ level, weakly allowed due to the hyperfine interaction and phonon-assisted mechanisms.

The spectrum of $KMgF_3$:Tl^+ at 300 K is a band with the maximum at 5.78 eV and a width of about 0.3 eV. This band does not disappear at 4.2 K; its maximum shifts to higher frequencies (5.91 eV) and an intensive narrow line at 5.812 eV is observed on its background.

The temperature-dependent luminescence decay was also investigated. At $T = 10$ K the lifetime of the slow component of luminescence is $\tau_s = 11.6$ ms for $KZnF_3$:Tl^+ and $\tau_s = 14.9$ ms for $KMgF_3$:Tl^+.

The main features of the observed luminescence spectra are satisfactorily explained within the framework of the conventional theory, as a manifestation of the Jahn–Teller effect for the excited 6sp electron configuration of an admixture Tl^+ ion, with a set of model parameters close to that used earlier to describe absorption spectra of the studied crystals.

1. Introduction

The present work is a continuation of our investigations of optical properties of the $KZnF_3$:Tl^+ and $KMgF_3$:Tl^+ crystals [1, 2]. These systems are interesting as promising materials for tunable lasers in the UV region. The $KMgF_3$:Tl^+ crystals are also known as good scintillators [3].

[1] Author to whom any correspondence should be addressed.

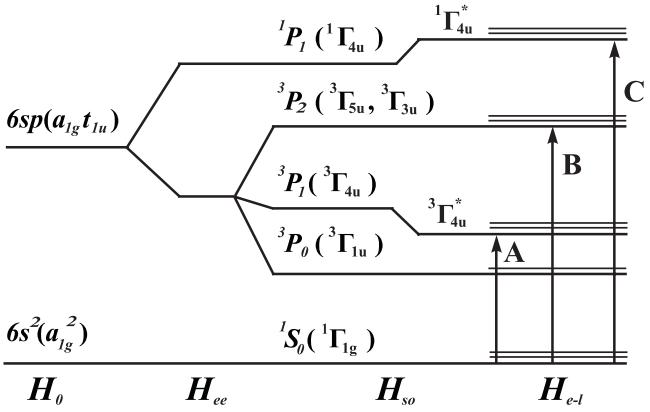

Figure 1. Energy levels of an s^2 ion in a crystal field of cubic symmetry.

The first investigations of absorption and photoluminescence of $KMgF_3$:Tl^+ crystals [4–6] have shown the similarity of those systems to alkali halide crystals doped with mercury-like ns^2 ions thoroughly studied earlier. This enables the description of the studied systems with a theory on the basis of the Frank–Condon principle, semi-classical theory of lattice vibrations and the Jahn–Teller theorem elaborated in detail and successfully used to interpret optical properties of alkali halide crystals (see reviews [7, 8]). In both types of crystal the Tl^+ ion occupies a position with cubic symmetry: in alkali halides the Tl^+ ion and its nearest surroundings form an octahedral complex of the $[TlF_6]^{5-}$ type; in fluoroperovskites the Tl^+ ion takes a position at the centre of a cube with apices occupied by Zn^{2+} (Mg^{2+}) ions and F^- ions located at centres of the cube edges. The cubic crystal field does not split electronic p states, so in the undistorted crystal an energy level scheme for $6s^2$, 6sp configurations ($(a_{1g})^2$, ($a_{1g}t_{1u}$) configurations in terms of molecular orbitals corresponding to s, p atomic orbitals) looks like that for a free Tl^+ ion (figure 1). Experimental values of E_A, E_B and E_C for the free ion equal 6.47, 7.68 and 9.38 eV, respectively. According to measurements of absorption spectra of KF:Tl^+ these values equal 5.42, 6.45 and 7.13 eV (see references to original works in a review [7]). The corresponding values for $KMgF_3$:Tl^+ [4] are 6.12, 7.38 and 8.27 eV, i.e., in this case the influence of the surroundings on the spectrum is essentially less than in alkali halide crystals.

Crystal lattice vibrations and the electron–vibration interaction give rise to the broadening of absorption and luminescence lines (formation of bands), to structuring of bands and to Stokes shifts. In [4] A, B and C absorption bands in the $KMgF_3$:Tl^+ crystal were observed and the temperature dependence of A and C bandshapes was measured. Proceeding from the temperature dependence of the band form functions, the authors estimated some parameters of the electron–vibration coupling. Those estimates are not very precise, due in part to the proximity of the impurity centre model. For Monte Carlo simulation of the absorption spectra [5] coupling parameters noticeably different from those given in [4] were used. The authors of [5] obtained a good agreement of the calculated spectrum with the one observed experimentally for $T = 10$ K. It should be noted, however, that calculations with the same parameters for higher temperatures lead to results strongly different from experiment.

In the previous work [1] we presented the results of investigating the A absorption band for two similar systems, $KZnF_3$:Tl^+ and $KMgF_3$:Tl^+, at temperatures of 10–300 K. For the second system our data practically coincided with the corresponding results of [4]. The A band in $KZnF_3$ is shifted by approximately 0.1 eV to lower energies compared to that in $KMgF_3$. We had chosen such sets of theoretical model parameters for both systems, which allowed us

to fit the calculated spectra and the observed ones in the whole temperature range. These sets differ from those used in [5]. In particular, the curvatures of parabolas describing adiabatic potentials in the ground ($6s^2$) and excited (6sp) configurations are approximately equal in our choice ($k_e \approx k_g = 1$), while in [5] the curvature is much larger for the excited states ($k_e = 2.1 \gg k_g = 1$).

The photoluminescence of the $KMgF_3:Tl^+$ system was originally investigated by authors of [6]. Under excitation in the A band (200 nm) at 20 K they observed an intensive luminescence band A′ ($E_{max} = 5.8$ eV (212 nm), half-width 0.27 eV) and a weak band with $E_{max} = 5.1$ eV (243 nm). As the temperature increased, the A′ band was broadened and shifted to lower energies. The decay of A′ luminescence was described by the sum of two exponents, a fast one with the decay time $\tau_f = 9$ ns at $T \leqslant 80$ K and a slow one with $\tau_s = 14$ ms at $T \leqslant 40$ K.

The luminescence spectra of $KZnF_3:Tl^+$ under excitation in the A band [2] essentially differ from those reported for $KMgF_3:Tl^+$ [6]. The main peculiarity is that at low temperatures an intensive narrow luminescence line is observed, which is due to zero-phonon transitions from the metastable level $^3\Gamma_{1u}$. Such a striking difference of luminescent properties for systems with highly similar absorption spectra prompted us to study in detail luminescence of the $KMgF_3:Tl^+$ crystal and to further investigate luminescence of the $KZnF_3:Tl^+$ crystal. As a result, it was clarified that indeed there are pronounced differences of luminescence spectra of the two studied systems; however, a narrow intensive zero-phonon line (ZPL) at low temperatures is present in spectra of both $KZnF_3:Tl^+$ and $KMgF_3:Tl^+$ systems.

In the present work the results of measurements and theoretical analysis of luminescence of the two mentioned systems are reported. In section 2 the crystal samples and apparatus are described. In section 3 the experimental results are given. In section 4 the luminescence model on the basis of the conventional theory of coupling of impurity ns^2 ions to the crystal surroundings is described. In section 5 the results of the model calculations are compared with experimental data. In conclusion the main results of the investigation are summarized.

2. Experimental procedure

$KZnF_3$ and $KMgF_3$ crystals doped with Tl^+ ions were grown by the Bridgman–Stockbarger method similarly to [1], the concentration of thallium ions in the melt being of about 0.5 wt%. It varied significantly (more than tenfold) along the pellet, which gave us the opportunity to prepare the samples with different thallium concentrations. The relative concentration of Tl^+ ions in the samples was estimated using the absorption spectra.

Luminescence and excitation spectra were measured under excitation by a high-pressure xenon lamp DKsEl-1000 with the use of an MDR-6 monochromator (in the excitation channel) and an MDR-23 monochromator (in the registration channel). The measured spectra were not corrected to the spectral response. The luminescence decay was studied upon excitation with a high-pressure xenon lamp DKSSh-150 operating in the pulse mode (pulse duration being of about 30 ns). The luminescence was detected by an FEU-106 photomultiplier tube working in the photon counting mode (the 'dead time' of the registration system was 0.2 μs). The separation of luminescence bands with different lifetimes was done by means of a phase-sensitive method [9]. For measurements in the temperature range of 4.2–300 K an Oxford Instruments CF-1204 optical cryostat was used.

3. Experimental results

3.1. $KZnF_3:Tl^+$

Upon excitation in the A absorption band (figure 2(a)) of $KZnF_3:Tl^+$ crystals [1, 2] at $T = 300$ K a wide luminescence band with $E_{max} = 5.48$ eV (figure 2(c)) is observed. This band reveals a

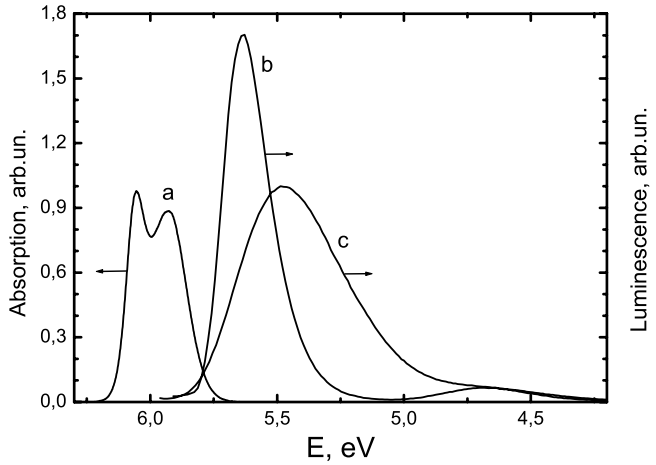

Figure 2. Absorption (a—300 K) and luminescence (b—100 K, c—300 K) spectra of the $KZnF_3$:Tl^+ crystal.

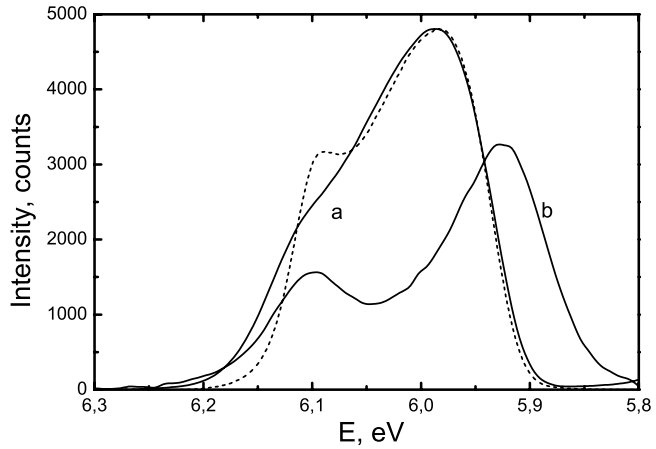

Figure 3. Excitation spectra (——) of the (A′ + A″) (a) and A_1 (b) luminescence bands and the absorption spectrum (- - - -, in arbitrary units) of the $KZnF_3$:Tl^+ crystal; $T = 100$ K.

shoulder at the low-energy side which transforms into an isolated luminescence band (A_1) with $E_{max} = 4.66$ eV, as the temperature decreases. Thus, the intense band and the weak A_1 band are observed at $T = 100$ K (figure 2(b)). We shall argue below that intensive luminescence is due to the interplay of two types of radiative transition: the electric-dipole-allowed transition $^3\Gamma^*_{4u} \rightarrow {}^1\Gamma_{1g}$ (A′) and the weakly allowed transition from the metastable level $^3\Gamma_{1u} \rightarrow {}^1\Gamma_{1g}$ (A″). Therefore the notation (A′ + A″) will mostly be used for intensive luminescence.

The excitation spectrum of the intense band at $T = 100$ K (figure 3(a)) almost coincides with the absorption spectrum (figure 3, dashed curve). This makes us suppose that the (A′ + A″) luminescence band corresponds to Tl^+ ions substituted for K^+ ions, which in the $KZnF_3$ crystal have only one regular crystallographic position. The formation of this type of doped Tl^+ centre is preferential due to the similar ionic radii of Tl^+ (1.44 Å) and K^+ (1.33 Å) ions.

The excitation spectrum of the A_1 luminescence band at $T = 100$ K (figure 3(b)) is close in energy to the A absorption band of Tl^+ ions but differs from the latter by the larger splitting

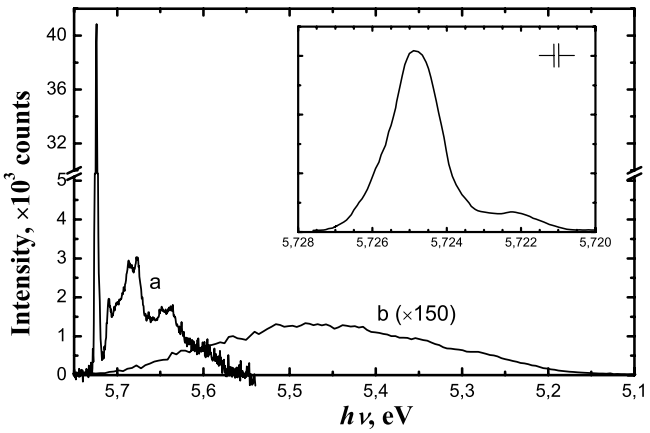

Figure 4. Luminescence spectrum of the $KZnF_3:Tl^+$ crystal at $T = 10$ K (a); spectrum of the fast, A′, luminescence component multiplied by a factor of 150 (b). The inset shows the resolved structure of the ZPL.

of the components of the doublet structure. This fact and the temperature dependence of the luminescence kinetics of the A_1 band (see below), which is typical for Tl^+ ions, show that the A_1 band also corresponds to Tl^+ ions, probably occupying some 'defect' positions. The investigations of the samples with different concentrations of thallium ions have shown that the ratio of A_1 and (A′ + A″) luminescence band intensities differs significantly in different samples but does not reveal any regular dependence.

At $T = 10$ K (figure 4) the wide intense band transforms into the sharp zero-phonon luminescence line with the corresponding vibronic structure. Close to the intense ZPL ($E_{max} = 5.7249$ eV) in the high-resolution spectrum (the inset of figure 4) a weaker sharp line with $E_{max} = 5.7222$ eV is observed. For temperature variation in the range of 4.2–30 K the ratio of intensities of these two lines is conserved. Thus the line with $E_{max} = 5.7222$ eV is the vibronic satellite of the ZPL and corresponds to the low-frequency mode (2.7 meV) in the ground state of the Tl^+ centre. It is possible also to derive from the observed vibronic structure of the luminescence spectrum the modes with frequencies of 9.9, 14.2 and 37.5 meV.

The temperature metamorphosis of the luminescence spectrum of the $KZnF_3:Tl^+$ crystal is shown in figure 5. As the temperature increases, the ZPL decreases in intensity and at $T > 120$ K only the wide structureless band is observed with the maximum shifted to the lower energies. The A_1 band remains structureless as the temperature decreases down to 10 K, only its width slightly decreases.

The temperature dependences of the decay time τ_s for the slow components of (A′ + A″) and A_1 luminescence bands are shown in figure 6. The lifetime of the (A′ + A″) band measured at $T = 10$ K is equal to about 11.6 ms, while the typical value of the fast luminescence lifetime (τ_f) at $T = 10$ K is of the order of 10 ns [6]. Such a big difference in the lifetime values has allowed us to measure the spectra of the fast and slow components by means of the phase-sensitive luminescence spectroscopy [9]. The rate of ${}^3\Gamma^*_{4u}$ state decay is rather high (see below), so the A′ component at low temperature may be conventionally considered as a fast component of (A′ + A″) luminescence. The weakly allowed transition ${}^3\Gamma_{1u} \rightarrow {}^1\Gamma_{1g}$ gives rise to a slow component A″. With the square-wave modulation of the excitation light at a frequency of 300 Hz and further lock-in luminescence signal detection with the phase of the excitation light, the spectrum of the slow component is suppressed about 10^3-fold compared to the spectrum

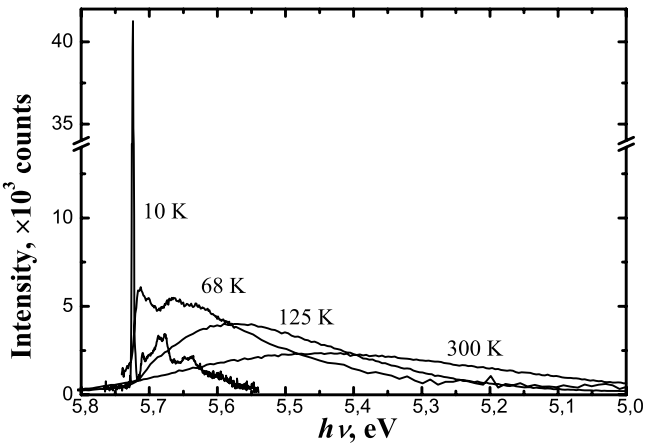

Figure 5. Temperature variation of the luminescence spectrum of the $KZnF_3:Tl^+$ crystal.

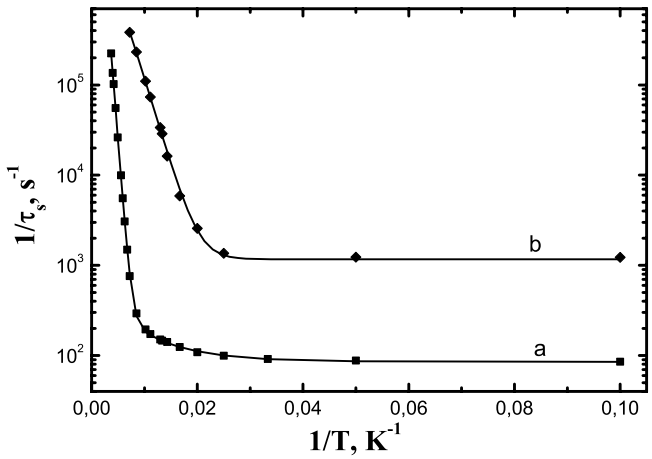

Figure 6. Temperature dependence of the slow component lifetime of the luminescence bands of the $KZnF_3:Tl^+$ crystal (a—for the $(A' + A'')$ band, b—for the A_1 band).

of the fast component (cf [10]). So with these experimental conditions the measured spectrum almost totally corresponds to fast luminescence (figure 4(b)). The measured ratio of integral intensities of the spectra of fast and slow components at $T = 10$ K is $I_{A'}/I_{A''} = 0.02$.

The temperature dependences of the lifetimes were analysed within a well known three-level model [8, 11], which is discussed in more detail in the next section. If the condition $k_1 \ll k_2 \ll k_{21}$ is fulfilled in the whole temperature range, then the temperature dependence of the slow component lifetime is described by the following equation [11] (cf also equation (16) below):

$$\tau_s^{-1} = \frac{k_1 + gk_2 \exp(-\Delta E/kT)}{1 + g \exp(-\Delta E/kT)}, \tag{1}$$

where k_1 and k_2 are the probabilities of the radiative transitions from levels 1 and 2, respectively, k_{21} is the probability of the nonradiative transition $2 \rightarrow 1$, g is the ratio of the degeneracy multiplicities of levels 2 and 1 (in our case $g = 2$) and ΔE is the energy gap between levels 1 and 2 (figure 11). The electric dipole radiative transition from metastable level 1 is forbidden

Table 1. Parameters of the three-level model defined from fitting the temperature dependences of the slow component lifetime for the $KZnF_3:Tl^+$ and $KMgF_3:Tl^+$ crystals.

	$KZnF_3:Tl^+$		
	A′ + A″	A_1	$KMgF_3:Tl^+$
$k_{10} + k_{1d}$ (s^{-1})	86 ± 1	1170 ± 20	67 ± 1
k_2 (s^{-1})	$(6.1 \pm 0.1) \times 10^7$	$(4.5 \pm 0.1) \times 10^6$	$(1.1 \pm 0.1) \times 10^8$
ΔE (meV)	147.2 ± 0.5	37.5 ± 0.5	201 ± 2
$\hbar\Omega$ (meV)	7.4 ± 2.2		13.8 ± 6.4
K (s^{-1})	$(3.1 \pm 0.1) \times 10^9$		$(4.3 \pm 0.1) \times 10^7$

and it becomes allowed due to different weak interactions (hyperfine interaction and phonon-assisted mechanisms; see the discussion). Equation (1) for τ_s^{-1} is well fitted to an experimental curve, if k_1 contains a temperature-dependent term as follows (cf [6]):

$$k_1(T) = k_{10} + k_{1d} \coth \frac{\hbar\Omega}{2kT}, \tag{2}$$

where Ω is interpreted as the vibration frequency in terms of the phonon-assisted mechanism and k_{1d} is the dynamic contribution to the probability at $T \to 0$. The fitting by equations (1) and (2) is shown in figure 6 by the solid curve; the values of the parameters are given in table 1. Separate terms k_{10} and k_{1d} are defined with high errors, so only the sum $(k_{10} + k_{1d})$ is given in the table. The value $K = k_{21}(T = 0)$ in table 1 is obtained using the following low temperature limit for ratio of the integral intensities of the A′ and A″ bands (cf equation (12) below):

$$I_{A'}/I_{A''} = k_2/k_{21} = k_2/K. \tag{3}$$

The probability k_{10} for the A_1 luminescence band is much greater than that for the (A′ + A″) band and the dynamic contribution can be neglected; the obtained values of the fitting parameters for this case are also given in table 1.

3.2. $KMgF_3:Tl^+$

As already mentioned in the introduction, the obtained experimental results on luminescence of the $KZnF_3:Tl^+$ crystal were found to be significantly different from those published earlier in [6] for the $KMgF_3:Tl^+$ crystal. Therefore we have studied in detail luminescence of the $KMgF_3:Tl^+$ crystal.

The absorption and luminescence spectra of the $KMgF_3:Tl^+$ crystal at $T = 300$ K upon excitation in the A absorption band are shown in figure 7. These spectra are shifted towards higher energies with respect to the spectra of $KZnF_3:Tl^+$, the Stokes shift at $T = 300$ K for the $KMgF_3:Tl^+$ crystal (0.326 eV) being noticeably smaller than that for $KZnF_3:Tl^+$ (0.512 eV).

The luminescence spectrum at $T = 6$ K (figure 8) consists of a wide vibronic band with $E_{max} = 5.91$ eV (A′) with a low-intensity ZPL at its high-energy edge ($E_{max} = 6.0307$ eV, see inset c in figure 8) and an intense ZPL ($E_{max} = 5.8123$ eV) with a vibrational structure (A″). The labelling of the luminescence bands corresponds to that for the $KZnF_3:Tl^+$ crystal; this assignment will be corroborated in the discussion. The temperature variation of the steady-state luminescence spectra of the $KMgF_3:Tl^+$ crystal is shown in figure 9.

The excitation spectra of the A′ band and of the intense ZPL A″ are identical and correspond to the A absorption band of the $KMgF_3:Tl^+$ crystal [1, 4]. This unambiguously proves that both luminescence components A′ and A″ are due to the same type of Tl^+ centre formed as in

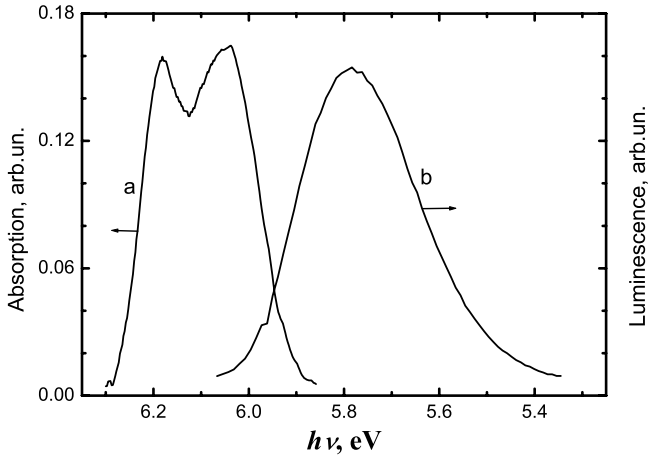

Figure 7. Absorption (a) and luminescence (b) spectra of the $KMgF_3$:Tl^+ crystal at $T = 300$ K.

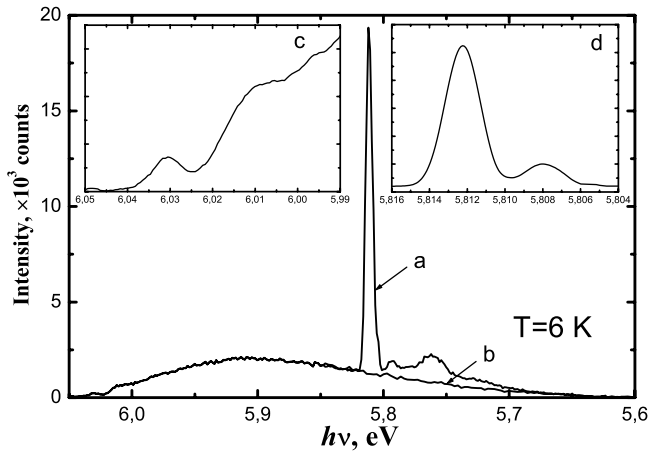

Figure 8. Luminescence spectrum of the $KMgF_3$:Tl^+ crystal at $T = 6$ K (a); spectrum of the fast component (b). Insets c and d show the high-resolution spectra in the regions of the ZPLs.

the $KZnF_3$:Tl^+ crystal by the substitution of K^+ ions with Tl^+ ions. It is necessary to note that no additional luminescence bands were found for the $KMgF_3$:Tl^+ crystal. The measurements of the fast and slow component spectra by the phase-sensitive method (figure 8(b)) have shown that at $T = 6$ K the A′ band corresponds to the fast component and the intense ZPL with a vibronic structure A″ to the slow component. The ratio of the integral intensities of A′ and A″ luminescence bands of the $KMgF_3$:Tl^+ crystal at $T = 6$ K is $I_{A'}/I_{A''} = 2.57$, the value being significantly larger than that for $KZnF_3$:Tl^+.

The analysis of the vibronic structure of the luminescence spectrum at $T = 6$ K (figure 8) allows us to define the vibrational mode with $\hbar\omega = 18.6$ meV appearing in vibronic structures of both A′ and A″ bands, and the modes with the frequencies 4.3 meV and 50.2 meV from the structure of the A″ band.

The temperature dependence of the slow component lifetime of Tl^+ ions in the $KMgF_3$ crystal is shown in figure 10. To analyse this dependence, the three-level model was used as for the case of $KZnF_3$:Tl^+. For the $KMgF_3$:Tl^+ crystal the condition $k_2 \ll k_{21}$ is not

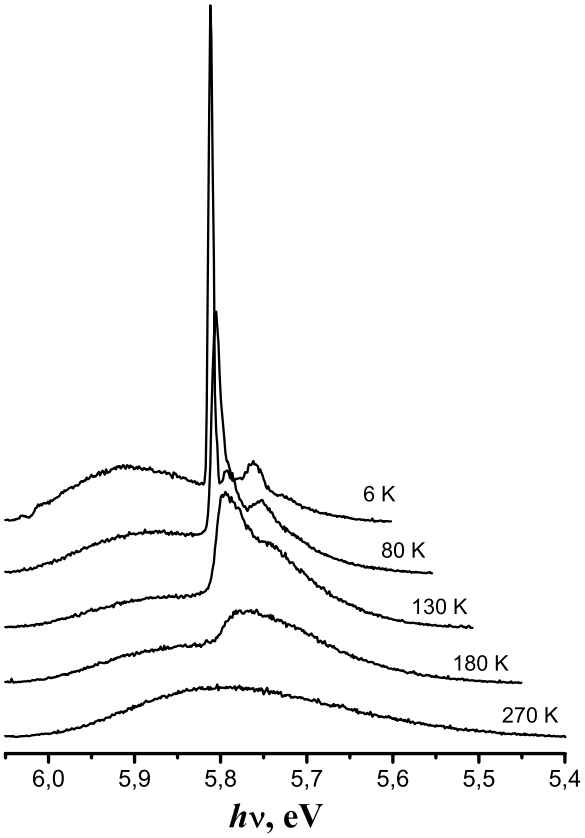

Figure 9. Temperature variation of the luminescence spectrum of the $KMgF_3:Tl^+$ crystal.

fulfilled because the value of $I_{A'}/I_{A''}$ is equal to 2.57. In this case expression (16) taking into account (17) should be used for the fitting. The fitting parameters are presented in table 1; the mean energy of the phonons which take part in the thermalization of states 1 and 2 (equation (17), figure 11) was found to be $\hbar\omega = 31.7 \pm 3.9$ meV. It should be mentioned that equation (16) used to fit the temperature dependence of the slow component lifetime of Tl^+ ions in the $KMgF_3$ crystal includes more parameters than in the case of $KZnF_3:Tl^+$ and this leads to a greater uncertainty of the parameter values.

4. Luminescence model

The model Hamiltonian is taken in the form typical for studies of optical centres formed by impurity s^2 ions, which occupy positions with cubic (or nearly cubic) symmetry in crystals:

$$H = H_0 + H_{ee} + H_{so} + H_{e-l}, \tag{4}$$

where H_0 corresponds to the single-electron approximation for a cubic quasimolecule composed of a Tl^+ ion and its nearest surroundings (one or two coordination spheres), H_{ee} is the Coulomb repulsion of electrons and H_{so} is the spin–orbit interaction. An energy level scheme (Seitz scheme [12]) for the ground and the first excited configurations of the system, which takes into account the Hamiltonian terms $H = H_0 + H_{ee} + H_{so}$, is given in figure 1. The kinetic energy of nuclei in equation (4) is omitted (adiabatic approximation). The term H_{e-l}

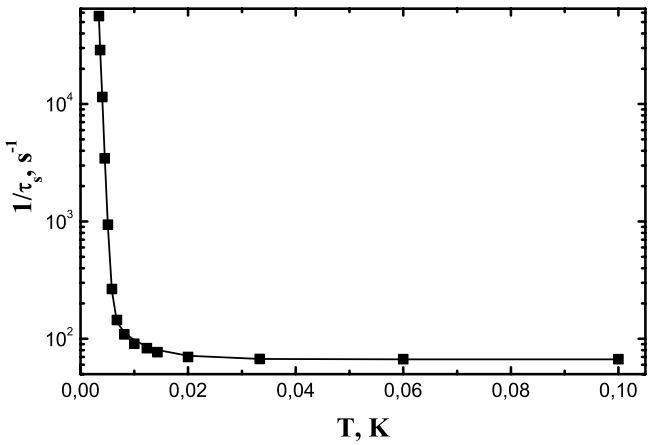

Figure 10. Temperature dependence of the slow component of the $KMgF_3:Tl^+$ crystal luminescence.

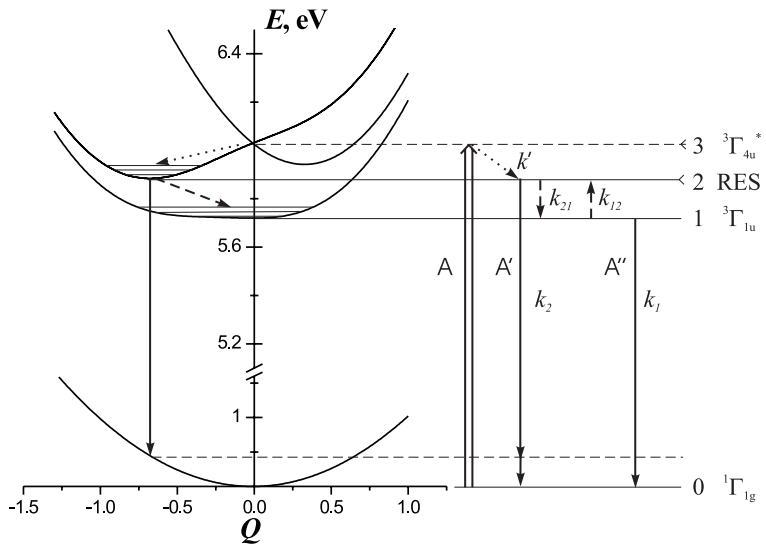

Figure 11. Cross-section of APESs of the thallium centre in the cubic surrounding, related to A absorption and subsequent luminescence.

includes the electron–vibration interaction in the first order and the elastic energy:

$$H_{e-l} = \sum V_i Q_i + \sum a_i Q_i^2. \tag{5}$$

Here Q_i are linear combinations of nuclear displacements from equilibrium positions, transforming in accordance with irreducible representations Γ_{1g}, Γ_{3g} and Γ_{5g} of the cubic group O_h. One may confine oneself to these representations, since only electronic operators V_i with corresponding symmetry properties have nonzero matrix elements on s, p (a_{1g}, t_{1u}) states of electrons. As mentioned before, it is possible to separate an octahedral complex of the $[TlF_6]^{5-}$ type in alkali halide crystals. For such a quasimolecule Q_1 (Γ_{1g}); Q_2, Q_3 (Γ_{3g}); Q_4, Q_5, Q_6 (Γ_{5g}) are normal coordinates of an octahedron, described already by Van Vleck [13]; a_i are elastic constants for corresponding normal vibrations, and each sum in

equation (5) contains six terms. Neither a change to another form of the nearest surroundings (e.g., $[TlF_{12}]^{11-}$ for systems studied in this paper), nor consideration of more distant neighbours of the impurity ion, results in an increase of the number of terms in the effective Hamiltonian of the electron–vibration interaction (see [1]). However, in these more general cases Q_i are not normal coordinates of a quasimolecule but the so-called 'interaction modes' [14] with the corresponding symmetry properties. Moreover, it is possible to take into account terms quadratic in Q_i without the complication of the Hamiltonian H_{e-l} and its matrix form by a change of the V_i and Q_i values (see equations (5) and (6) in [1]). However, such consideration does not lead to essentially new qualitative results, and we shall confine ourselves to the interaction of electrons with the crystal lattice linear in nuclear displacements in order not to increase the number of model parameters. Q_1 is called a fully symmetric mode, Q_2, Q_3 (Γ_{3g}) are tetragonal modes (for instance, $Q_3 \neq 0$ corresponds to elongation or contraction of a quasimolecule along one of the fourfold axes) and Q_4, Q_5, Q_6 (Γ_{5g}) are trigonal modes ($Q_4 = Q_5 = Q_6$ leads to the distortion along the trigonal axis).

An equilibrium nuclear configuration for the ground electron state is chosen as an origin for displacements Q_i, therefore the first term in equation (5) turns to zero in the ground electron configuration. As usual, the scale of Q_i is chosen in such a way that the elastic energy in the ground state has a form $\langle H_L \rangle_g = \sum Q_i^2$ ($\dim Q = \text{energy}^{1/2}$). Thus the energy $E_g(Q)$ of the ground state is a six-dimensional rotation paraboloid. For the excited configuration

$$H_L^{exc} = a_1 Q_1^2 + a_2(Q_2^2 + Q_3^2) + a_3(Q_4^2 + Q_5^2 + Q_6^2). \tag{6}$$

Coefficients a_1, a_2 and a_3 take into account the possible difference of effective elastic constants (and corresponding effective frequencies) for the ground and excited configurations. In [5, 8] the notation k_e is used, $k_e \equiv a_1 = a_2 = a_3$.

When perturbation (5) is taken into account, the excited levels E_A, E_B and E_C (see figure 1) are split, and a complicated picture of 12 adiabatic potential-energy surfaces (APESs) $E_n(Q_1, \ldots, Q_6)$ emerges. Minima of these potentials are the so-called 'relaxed excited states' (RESs), to which the optical centres go over after excitation and thermal relaxation, as an intermediate stage of luminescence. Figure 11 shows the cross-section of the APES by a plane corresponding approximately to the trigonal distortion ($Q_1 = Q_2 = Q_3 = 0$, $Q_4 = Q_5 = Q_6$). The APES was calculated with the parameters (26) and (27) for the $KZnF_3:Tl^+$ crystal. Potential energies for the ground state $^1\Gamma_{1g}$ and four lower excited states coupled to unperturbed terms $^3\Gamma_{1u}$ and $^3\Gamma_{4u}^*$ are presented schematically. The mentioned states take part in forming an A absorption band and the corresponding A′ and A″ luminescence bands. Several minima are shown in figure 11; the bottom of the upper parabola is not a minimum with respect to other coordinates and therefore it is not an RES.

The general picture of the phenomenon may be presented as follows (see figure 11). Excitation of centres takes place in a comparatively small range of Q values, corresponding to fluctuations of lattice deformations in the ground electronic state within the limits of $Q_i^2 \sim kT_i^*$. An effective temperature T_i^* is defined approximately by the mean-square fluctuation

$$kT_i^* = 2\langle Q_i^2 \rangle = (\hbar\omega_i/2)\coth(\hbar\omega_i/2kT), \tag{7}$$

where ω_i is the effective frequency coupled to the ith interaction mode. Under pumping in the A band the triplet $^3\Gamma_{4u}^*$-states with energies near E_A are populated. As a result of the distortion of the excited quasimolecules, optical centres 'slide' along the APES to positions near minima (this shifting to the RES is shown in figure 11 by dotted arrows). The RES may decay due to radiative transitions into the ground state, or, as a result of non-radiative transitions, to other minima of adiabatic potential energies (the last transitions are shown in figure 11 by broken lines).

The Hamiltonians (4) and (5) are invariants of the O_h group, i.e., they turn into themselves under all transformations of this group, applied simultaneously both to electron coordinates and to nuclear variables Q_i. Therefore the multifold function $E_n(Q)$ in the six-dimensional space Q_i is also a cubic invariant:

$$E_n(Q_i) = E_n[Q_i' = D(g)Q_i], \tag{8}$$

where Q_i is an arbitrary point in the space of displacements and $D(g)$ is an operator of the (reducible) representation of the O_h group in this space, corresponding to a group element g. The symmetry of functions E_n in some cases may be higher than cubic. Thus, the adiabatic potential energy for the ground state $^1\Gamma_{1g}$ is symmetric with respect to all rotations and reflections in the six-dimensional space of displacements. Under operations of the O_h group all points of an axis Q_1 transform into themselves; all points of the (Q_2, Q_3) plane are invariant with respect to the subgroup $D_{2h} \subset O_h$, and in this plane the group O_h reduces to the C_{3v} factor group with Q_3 as one of the reflection axes. Therefore the function $E_n(Q_2, Q_3)$ possesses the trigonal symmetry in the plane Q_2, Q_3. The function $E_n(Q_4, Q_5, Q_6)$ has a tetrahedral symmetry. We recall that all Q_i belong to even representations, i.e., they are invariant under inversion. All said above about the symmetry of functions E_n also refers to the system of extrema of these functions and to the equipotential surfaces.

The kinetics of the processes shown in figure 11 is described approximately by the following system of balance equations for populations of energy levels denoted by indices 0, 1, 2 and 3, respectively, for the ground state $^1\Gamma_{1g}$, the metastable state $^3\Gamma_{1u}$, the RES related to the triplet $^3\Gamma^*_{4u}$ and unrelaxed states of this triplet, excited by the external source of light:

$$\begin{aligned}
\dot{N}_1 &= -(k_1 + k_{12})N_1 + k_{21}N_2, \\
\dot{N}_2 &= k_{12}N_1 - (k_2 + k_{21})N_2 + k'N_3, \\
\dot{N}_3 &= -(W' + k')N_3 + WN_0, \\
\dot{N}_0 &= k_1N_1 + k_2N_2 + W'N_3 - WN_0,
\end{aligned} \tag{9}$$

where k_1 and k_2 are probabilities of spontaneous radiation from levels 1 and 2, related to the time unit; k_{12}, k_{21} are probabilities of nonradiative transitions between levels 1 and 2; W is the probability of the transition $^1\Gamma_{1g} \rightarrow {}^3\Gamma^*_{4u}$, induced by the external source, and defining the A absorption band; W' is the probability of the reverse transition and, finally, k' is the velocity of sliding of an excited centre to relaxed states. The value of $\tau' = k'^{-1}$ may be roughly estimated as a mean period of a quasimolecule oscillation about an equilibrium position near the minimum of the adiabatic potential energy. Effective frequencies of oscillations are usually of the order of 10–100 cm^{-1}, so $\tau' \leqslant 10^{-12}$ s which is essentially less than radiation lifetimes $\tau_{rad} \sim 10^{-2}$–10^{-9} s and typical lifetimes for nonradiative transitions ($\tau_{nrad} \geqslant 10^{-10}$ s). Nonradiative transitions between levels 1 and 2 result in thermal equilibrium, therefore the velocities of these transitions are related by the following equation:

$$k_{12} = gk_{21}\exp(-\Delta E/kT), \tag{10}$$

where ΔE is an energy interval between levels 1 and 2 and g is the ratio of degeneracy multiplicities for levels 2 and 1 ($g = 2$ for the scheme in figure 11).

Under the stationary excitation of luminescence ($\dot{N} = 0$) equations (9) are solved as follows:

$$\begin{aligned}
N_1^0 &= \frac{k_{21}k'}{k_1k_{21} + k_2k_{12} + k_1k_2}N_3^0, \qquad N_2^0 = \frac{(k_1 + k_{12})k'}{k_1k_{21} + k_2k_{12} + k_1k_2}N_3^0, \\
N_3^0 &= \frac{W}{W' + k'}N_0^0.
\end{aligned} \tag{11}$$

It is seen that $N_2^0/N_1^0 = (k_1 + k_{12})/k_{21}$, and intensities of the A′ and A″ luminescence bands are related as follows:

$$I_{A'}/I_{A''} = k_2 N_2^0/k_1 N_1^0 = k_2(k_1 + k_{12})/k_1 k_{21} = (k_2/k_{21}) + (k_2/k_1)\exp(-\Delta E/kT). \tag{12}$$

The decay of luminescence after switching off the exciting source ($W' = W = 0$) is governed by the first three equations of the system (3). The first stage of the process, the decay of the level 3 [$N_3(t) = N_3(0)\exp(-t/\tau')$], proceeds within a very short time τ' which is not measured in usual observations. Consequently the observed kinetics reduces to the first two equations in (9) with $N_3 = 0$, which are usually written down in the literature (see [6, 8, 11]). The initial conditions for these equations at not very short excitation pulses are the following: $N_1(0) = N_1^0$, $N_2(0) = N_2^0 + N_3^0$. The luminescence decay is described by two exponents,

$$N_i = A_i \exp(-t/\tau_f) + B_i \exp(-t/\tau_s), \qquad i = 1, 2;\ A_i + B_i = N_i(0), \tag{13}$$

where the lifetimes $\tau_{f,s}$, corresponding to the fast and slow decay modes, look as follows:

$$\begin{aligned} &\tau_{f,s}^{-1} = \tfrac{1}{2}(k_1 + k_2 + k_{21} + k_{12}) \pm D^{1/2}, \\ &D = \tfrac{1}{4}(k_2 + k_{21} - k_1 - k_{12})^2 + k_{12}k_{21}, \\ &\tau_f^{-1}\tau_s^{-1} = k_1 k_{21} + k_2 k_{12} + k_1 k_2. \end{aligned} \tag{14}$$

At very low temperatures $k_{12} \to 0$; then

$$\tau_f^{-1} = k_2 + k_{21}, \qquad \tau_s^{-1} = k_1. \tag{15}$$

For higher temperatures one may use the following approximate relations:

$$\begin{aligned} &\tau_f^{-1} = k_2 + k_{21}[1 + gr\exp(-\Delta E/kT)], \\ &\tau_s^{-1} = \frac{k_1 + gk_2 r\exp(-\Delta E/kT)}{1 + gr^2\exp(-\Delta E/kT)}, \\ &r = \frac{k_{21}}{k_{21} + k_2}. \end{aligned} \tag{16}$$

If $k_{21} \gg k_2$, then $r \approx 1$, and equations (16) are simplified yet more (see equation (2)). In this case the lifetime τ_s does not depend on the specific mechanism of nonradiative transitions. Usually these transitions are due to processes with production and annihilation of phonons. If the transition $2 \to 1$ is accompanied by production of p phonons with the frequency ω ($p \approx \Delta E/\hbar\omega$), then (see [6])

$$k_{21} \approx K(n+1)^p, \qquad n = \left(\exp\frac{\hbar\omega}{kT} - 1\right)^{-1}, \tag{17}$$

where $K = k_{21}(0)$ does not depend on temperature. The value $k_{21}(T)$ increases rapidly with temperature, $k_{21} \sim T^p$ at $kT > \hbar\omega$, therefore the above condition $k_{21} \gg k_2$ takes place at least for high enough temperatures.

Concerning mechanisms of radiative transitions, the transition ${}^1\Gamma_{1g} \leftrightarrow {}^3\Gamma_{4u}^*$ is known as an allowed electric dipole one [7, 8]. Due to the spin–orbit interaction the ${}^3\Gamma_{4u}^*$ triplet states are mixtures of Russel–Saunders terms with spins $S = 1$ and 0:

$$|{}^3\Gamma_{4u}^*, i\rangle = \mu|{}^3\Gamma_{4u}, i\rangle - \nu|{}^1\Gamma_{4u}, i\rangle \tag{18}$$

and the admixture of ${}^1\Gamma_{4u}$ states makes the transition allowed. The spin–orbit interaction in a heavy Tl^+ ion is rather strong, so the mixing of ${}^3\Gamma_{4u}$ and ${}^1\Gamma_{4u}$ states is essential. The degree of mixing is defined by the parameter $R = \mu^2/\nu^2$, which in alkali halides is estimated as $R \approx 4$–5 [7, 8]. The estimates of R value in $KMgF_3:Tl^+$ are approximately the same [4].

The deformation of the Tl^+-containing complex, due to the nuclear motion, leads to the further mixing of the excited configuration states. Already in the first order on any non-fully-symmetric deformation the triplet states Γ_{4u} are mixed to the states (${}^3\Gamma_{3u}$, ${}^3\Gamma_{5u}$), and transitions

leading to the B absorption band become allowed. The triplet states $^3\Gamma^*_{4u}$, $^1\Gamma^*_{4u}$ do not admix to the metastable state $^3\Gamma_{1u}$ in either the first or second order of the perturbation theory, so the usual electron–vibration mechanism is not effective for allowing the transition $^1\Gamma_{1g} \leftrightarrow {}^3\Gamma_{1u}$.

However, the magnetic field mixes the states $^3\Gamma_{1u}$ and $^3\Gamma_{4u}$. Matrix elements of angular moment operators are as follows (cf [8]; we use functions $|^3\Gamma_{4u}, \alpha\rangle$, which differ from those in [8] by a factor i [1, 14]):

$$\langle {}^3\Gamma_{1u}| \sum (l_z + 2s_z)|^3\Gamma_{4u}, z\rangle = 2\sqrt{\tfrac{2}{3}}(1 + \tfrac{1}{2}g_0), \tag{19}$$

where $g_0 = i\langle a_{1x}|l_z|a_{1y}\rangle$, and for pure atomic orbitals ($a_{1x} = p_x$) $g_0 = 1$. Energy intervals between $^3\Gamma^*_{4u}$ and $^3\Gamma_{1u}$ levels are of the order of several tenths of electron volts, and in the conventional magnetic fields of about 1 T the admixture coefficient is very small, less than 10^{-4}. However, internal magnetic fields due, for instance, to magnetic moments of nuclei, may reach significant values.

The hyperfine interaction as an origin of optical transitions $^3\Gamma_{1u} \leftrightarrow {}^1\Gamma_{1g}$ in thallium-doped compounds was proposed for consideration by authors of [15, 16]. The Hamiltonian of the hyperfine interaction is as follows [17]:

$$H_{hf} = 2\mu_B\gamma_n \boldsymbol{I} \cdot \sum \left\{ \frac{\boldsymbol{l} - \boldsymbol{s}}{r^3} + 3\frac{\boldsymbol{r}(\boldsymbol{s}\cdot\boldsymbol{r})}{r^5} + \frac{8\pi}{3}\boldsymbol{s}\delta(r) \right\}, \tag{20}$$

where $\boldsymbol{I}$ is a nuclear spin and γ_n is a nuclear gyromagnetic ratio. The hyperfine interaction of s electrons is defined mainly by the last term (contact interaction) in equation (20), and this term by far exceeds interactions of other electrons with a nucleus. The contact hyperfine interaction of a separate s electron after averaging over orbital variables can be written as a spin Hamiltonian:

$$H^c_{hf} = A\boldsymbol{I}\cdot\boldsymbol{s}, \qquad A = \frac{16\pi}{3}\mu_B\gamma_n R^2_{6s}(0), \tag{21}$$

where $\boldsymbol{s}$ is an electron spin and $R_{6s}(r)$ is an electron 6s function of the Tl^+ ion. The matrix elements of the contact part of H_{hf} between the states ($^1\Gamma_{4u}$, $^3\Gamma_{4u}$) and $^3\Gamma_{1u}$ look as follows:

$$\langle {}^1\Gamma_{4u}, z|H^c_{hf}|^3\Gamma_{1u}\rangle = \frac{1}{2\sqrt{3}}AI_z, \qquad \langle {}^3\Gamma_{4u}, z|H^c_{hf}|^3\Gamma_{1u}\rangle = -\frac{1}{\sqrt{6}}AI_z, \tag{22}$$

i.e., x, y, z-states of triplets Γ_{4u} are admixed to the state $^3\Gamma_{1u}$ equally. An admixture coefficient for each nuclear magnetic state may be approximately estimated as follows:

$$|^3\Gamma_{1u}\rangle \to |^3\Gamma_{1u}\rangle + \frac{A}{E_A - \mathrm{E}(^3\Gamma_{1u})}|^3\Gamma^*_{4u}\rangle. \tag{23}$$

Another 'magnetic' mechanism of allowing the transition $^1\Gamma_{1g} \leftrightarrow {}^3\Gamma_{1u}$ was discussed in detail by Asano [18]. A rotation of charged particles surrounding the Tl^+ ion gives rise to a magnetic field at the ion location. The rotations within crystals have a character of random rotational oscillations, which for the cubic surroundings relate to Γ_{4g} symmetry modes. The Hamiltonian of electron–vibration coupling, corresponding to the considered mechanism, can be represented in the following form:

$$H'_{e-l} = \sum F(\boldsymbol{r})(\boldsymbol{l} + 2\boldsymbol{s})\cdot\dot{\boldsymbol{Q}}, \tag{24}$$

where the summation is carried out over two electrons of s^2 and sp configurations and Q_x, Q_y and Q_z are the rotational coordinates composed from nuclear displacements (for an octahedral complex TlF_6 these are simply rotational coordinates Q_{19}, Q_{20} and Q_{21} [13]). A dot over $\boldsymbol{Q}$, as usual, stands for differentiation over time. The mechanism is non-adiabatic and electron operators in (24) change their sign under time reversal. Such operators having a symmetry

mode $\Gamma_{4g} = \{\Gamma^2_{4u}\}$ have nonzero matrix elements on p electronic states. There are also other non-adiabatic mechanisms of electron–vibration coupling [19], which were considered as a possible reason for the anomalous temperature dependence of the spin–lattice relaxation time in K_2SO_4:Tl^{2+}, observed in [20]. An effectiveness of state mixing due to non-adiabatic mechanisms increases with temperature, similar to other mechanisms with participation of phonons.

Now we turn to discussion of the experimental results.

5. Discussion

The luminescence in alkali halide crystals containing impurity s^2 ions is usually analysed by considering the APES $E_n(Q_2, Q_3)$ in the space of tetragonal displacements (see [7, 8]). This restriction greatly simplifies the theoretical analysis and makes it very clear; however, the direct comparison of such analysis with experiment is evidently possible only if a coupling to tetragonal modes Q_2 and Q_3 prevails in electron–vibration interaction, when the parameter b is great, $|b| > |c|$. The coupling parameters are defined as follows [1] (only the second term of a is given in [8]):

$$\begin{aligned} a &= \langle \mathrm{a_{1g}}|V_1|\mathrm{a_{1g}}\rangle + \langle \mathrm{t_{1u}}, x|V_1|\mathrm{t_{1u}}, x\rangle, \\ b &= \langle \mathrm{t_{1u}}, x|V_2|\mathrm{t_{1u}}, x\rangle, \\ c &= \langle \mathrm{t_{1u}}, y|V_4|\mathrm{t_{1u}}, z\rangle. \end{aligned} \tag{25}$$

In principle, single-electron radial functions differ for triplet (summary spin $S = 1$) and singlet ($S = 0$) states of the sp configuration. To take into account this circumstance, the matrix elements a', b' and c' for single-electron wavefunctions referring to the singlet $S = 0$ are considered as independent parameters, different from those (a, b and c) for triplet states.

An analysis of absorption spectra in $KMgF_3$:Tl^+ and $KZnF_3$:Tl^+ systems has shown that in these systems an interaction with trigonal modes Q_4, Q_5 and Q_6 prevails: $|c| > |b|$ [1, 5]. In such a case it is natural to investigate minima of functions $E_n(Q_4, Q_5, Q_6)$ in three-dimensional subspaces of trigonal displacements as an initial approximation. These minima should be deeper than tetragonal ones. We have carried out these calculations for systems $KZnF_3$:Tl^+ and $KMgF_3$:Tl^+ on the basis of parameters of the energy matrix for the excited sp-configuration of the impurity centre obtained in the previous work [1]. For the first system we assume

$$\begin{aligned} &E_1(^3\Gamma_{1u}) = 5.72\ \mathrm{eV}, \qquad E_A = 6.03\ \mathrm{eV}, \\ &E_B = 7.2\ \mathrm{eV}, \qquad E_C = 8.14\ \mathrm{eV}. \end{aligned} \tag{26}$$

Here E_A, E_B and E_C are the mean positions of the corresponding absorption bands; E_1 coincides approximately with the position of the ZPL. Parameter R, defining the mixing of spin triplet and singlet states by the spin–orbit interaction, and parameters of electron–vibration interaction (in eV) are as follows:

$$\begin{aligned} &R = 7, \qquad c^2 = 1.69, \qquad c'^2 = 1, \qquad a^2 = a'^2 = 0.023, \\ &b^2 = 0.49, \qquad b'^2 = 0.25. \end{aligned} \tag{27}$$

Elastic constants a_i in equation (6) were assumed to be equal to unity. When only trigonal distortions of the impurity surroundings are considered, parameters a, a', b and b', of course, do not enter into calculations. However, they are used to estimate the influence of other vibration modes on preliminary results.

The triplet $E(^3\Gamma^*_{4u})$ is unfolded to a three-sheeted surface in the space of displacements. Figure 12 shows contours of the lower sheet of the surface in the plane (Q_6, $Q_4 = Q_5$), containing the trigonal axis $Q_4 = Q_5 = Q_6$ (tr). Minima T with $E_T = 5.88$ eV are clearly

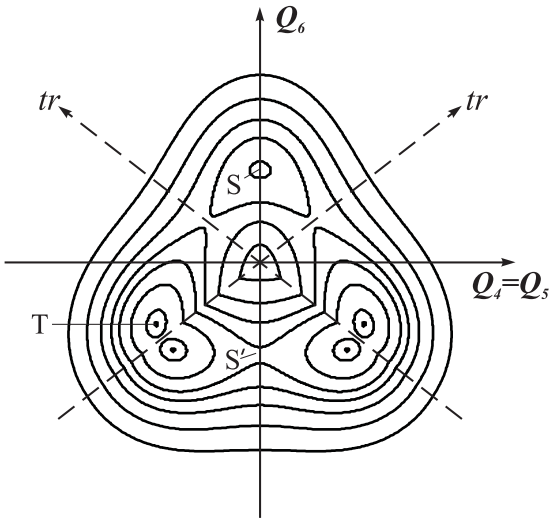

Figure 12. Contours of the lower sheet of the three-sheeted surface $E(^3\Gamma^*_{4u}; Q_4, Q_5, Q_6)$. The lines of equal energy are projected on the plane (Q_6, $Q_4 = Q_5$).

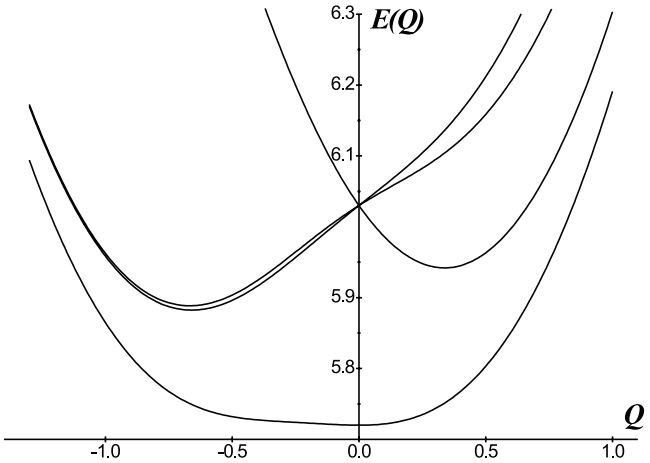

Figure 13. APES of the excited states $^3\Gamma_{1u}$ and $^3\Gamma^*_{4u}$. The cross-sections by the plane containing the direction to a minimum (T) of the lower sheet of the surface $E(^3\Gamma^*_{4u}, Q)$ is drawn.

seen; in fact, there are four series of equivalent minima grouping near the trigonal axes. The point S with $E_S = 5.95$ eV is a saddle point equivalent to the point S'. In figure 13 cross-sections of APES connected to the triplet $^3\Gamma^*_{4u}$ and the singlet $^3\Gamma_{1u}$, in the plane containing the direction to the minimum T, are drawn.

The splitting of the trigonal doublet, arising from the triplet $^3\Gamma^*_{4u}$, in the point T is comparatively small ($\sim$0.02 eV), groups of close minima, relating to one series, nearly coincide, and to simplify the discussion one can reasonably consider them as a single trigonal minimum. The lower optically inactive state $^3\Gamma_{1u}$ of the excited sp configuration has a weakly pronounced minimum of energy at $Q = 0$: $E(^3\Gamma_{1u}, Q = 0) = 5.72$ eV. The cross-section of APES in the direction of the trigonal deformation of a quasimolecule (along the tr-axis) is schematically shown in figure 11, and it has already been used to formulate a model. As is evident, there are

sufficient grounds to make use of the luminescence model formulated in the previous section. According to this model, we identify an intensive luminescence band at 5.48 eV observed at room temperature with the A′ band in figure 11, caused by transitions from relaxed states, corresponding to the T-minimum, to the ground state with the same value of the displacement $Q = Q_T$ (the Frank–Condon principle). The mean value of the transition energy, obtained as a result of calculations,

$$E_{A'} = E_{RES}({}^3\Gamma^*_{4u}, Q_T) - E_g({}^1\Gamma_{1g}, Q_T) \cong 5.9 - Q_T^2 = 5.5\,\text{eV} \tag{28}$$

approximately conforms to the observed location of the A′ band. The calculated value of $\Delta E = E_{RES}({}^3\Gamma^*_{4u}, Q_T) - E_1({}^3\Gamma_{1u}, Q = 0) \approx 0.16$ eV (see figures 11 or 13) conforms rather well to that found experimentally (0.147 eV, table 1).

The A′ band has a significant width even at low temperatures. The final state of the transition falls within the abrupt segment of a paraboloid representing the adiabatic potential energy of the ground level ${}^1\Gamma_{1g}$. Even small fluctuations δQ about the value Q_T in the initial state, which exist at any temperature, lead to an essential spread of final energies and therefore to noticeable bandwidth. At temperatures exceeding the quantum $\hbar\omega'$ of the vibration energy of impurity centres in the RES, the bandwidths can be roughly estimated as follows:

$$|\Delta E_{A'}| \approx 2Q_T\delta Q \approx 2Q_T\sqrt{\frac{kT\omega_3}{2\omega'}} \approx 10^{-2}\sqrt{\frac{\omega_3}{\omega'}T}\ \text{eV}, \tag{29}$$

where temperature T is measured in Kelvin, $\omega_3 = \omega(\Gamma_{5g})$ is the frequency corresponding to trigonal displacements in the ground electronic state and ω' is the effective oscillation frequency in the RES. Earlier we estimated the frequency ω_3 as $\omega(\Gamma_{5g}) \approx 100\ \text{cm}^{-1}$ [1]; the curvature of the adiabatic potential energy near the minimum T is much less than the curvature of the parabola Q^2, i.e., $\omega(\Gamma_{5g}) \gg \omega'$ (see figure 13). Supposing an effective frequency ω' of about $10\ \text{cm}^{-1}$, one obtains a satisfactory agreement of formula (29) with experimental data.

An intensive narrow line at 5.7249 eV, observed at low temperatures, is ascribed to the A″ transition (figure 11) from the metastable state 1 (${}^3\Gamma_{1u}$) to the ground state 0. After pumping in the A band and transition to the RES near points T of the configuration space Q, one fraction of the optical centres radiates in the A′ luminescence band. Another fraction crosses to the singlet state ${}^3\Gamma_{1u}$, sliding back down to the vicinity of the Q-space origin, which also corresponds to the minimum energy of the ground state ${}^1\Gamma_{1g}$. (Here we confine ourselves to trigonal displacements Q_4–Q_6. A consideration of a fully symmetric displacement results in a shift of the minimum position of the metastable state along Q_1. The shift is evidently very small due to the small value of the electron–vibration coupling parameter a.) At low temperatures ($T \leqslant 10$ K) the centres localize near the immediate vicinity of an origin $Q = 0$, and under such conditions the classic description of impurity centre oscillations, as a motion along the APES, becomes insufficient.

The transitions ${}^3\Gamma_{1u} \rightarrow {}^1\Gamma_{1g}$ lead to the narrow ZPL with a large peak intensity and to vibration satellites, for which the transition is accompanied by producing one or more phonons in the ground electron state. Our measurements allow us to establish the presence of pronounced vibrations with frequencies of 22, 80, 115 and 300 cm^{-1}. We do not have enough data for an unambiguous identification of these vibrations. The frequencies 115 and 300 cm^{-1} correlate well with effective frequencies $\omega(\Gamma_{5g}) = 100\ \text{cm}^{-1}$ and $\omega(\Gamma_{3g}) = 300\ \text{cm}^{-1}$ used in [1]. One of the lower frequencies is probably related to the pseudolocal vibration, due to the substitution of the K^+ ion by the heavy Tl^+ ion, while the other may be referred to the libration Γ_{4g} mode. The frequency of the pseudolocal vibration may be roughly estimated as follows (see, e.g., [21]):

$$\omega_{pseud} = \omega_{Deb}/\sqrt{3m/m'}, \tag{30}$$

where m and m' are atomic masses of Tl and K, respectively ($m/m' = 5$).

The minimum of the surface $E(^3\Gamma_{1u}; Q)$ is weakly pronounced (figure 13), and as the temperature increases, the fluctuations of Q in this state rapidly grow. The ZPL and its satellites are broadened, and its peak is shifted to the lower frequencies as usual [21]. At $T \approx 100$ K the value of δQ can be approximately estimated as 0.4 (figure 13), which results in the width of the order of $Q^2 = 0.16$ eV, and the ZPL becomes unobservable, in full accord with experiment. This is favoured also by the fact that as the temperature increases, the probability of reverse transitions from the metastable state (1) to the RES (2) grows. A fraction of optical centres make such transitions and then radiate from the RES into the A′ band, thus diminishing the integral intensity of the A″ radiation. The observed luminescence band for $T \geqslant 100$ K is a superposition of the A″ and A′ bands; as the temperature increases, the role of A′ increases and the maximum of the whole band shifts to lower energies, to the position of the A′ band.

The slow luminescence kinetics was measured in our experiments. At low temperatures the corresponding luminescence decay time τ_s is equal, according to equation (15), to the radiation lifetime k_1^{-1} of the metastable state. The experimental value is $k_1 = 86$ s^{-1} (see figure 6 and table 1). At low temperatures $k_{12} \to 0$ and, according to equation (12), $I_{A'}/I_{A''} = k_2/k_{21} = 0.02$ (for $T = 10$ K). As the temperature increases, the value of k_{21} may only grow (cf equation (17)), therefore the condition $k_{21} \gg k_2$ in this case holds over the whole temperature range, and equations (16) with $r = 1$ (i.e., equation (1)) for decay times can reliably be used. This means that the value of the energy interval ΔE is defined by the slope of the exponential part of the function $\tau_s^{-1}(T^{-1})$ in figure 6 ($\Delta E \approx 147$ meV, table 1) and k_2 is approximately defined by the intersection of that part with the ordinate axis ($k_2 \approx 6 \times 10^7$ s^{-1}). The nonradiative transition coefficient is equal to $k_{21}(0) = K = 50k_2 = 3 \times 10^9$ s^{-1}. The intensity ratio $I_{A'}/I_{A''}$, as seen in equation (12), increases with temperature.

The rates of radiation transitions from the metastable state $^3\Gamma_{1u}$ and RES $^3\Gamma^*_{4u}$ are related as $k_1/k_2 \approx 1.4 \times 10^{-6}$, which is consistent with the admixture coefficient of $^3\Gamma^*_{4u}$ states to $^3\Gamma_{1u}$ due to hyperfine interaction (see equation (23)) obtained in the previous section. The hyperfine interaction parameter A for thallium is equal to about 2 cm^{-1} (cf [15]), the energy interval $E_A - E_1 \approx 0.3$ eV (at $Q = 0$), therefore $A^2/(E_A - E_1)^2 \approx 10^{-6}$, which is equal to k_1/k_2.

Equation (16) with the above values of k_1, k_2 and ΔE describes the experimental temperature dependence well, except for the temperature range of $25\text{ K} < T < 100$ K, corresponding to the salient point of the curve. Probably, phonon-assisted mechanisms of the radiation transition $^3\Gamma_{1u} \to {}^1\Gamma_{1g}$ (e.g., those described at the end of the previous section) are responsible for this discrepancy. They can be roughly taken into account by inclusion of a temperature-dependent term into the radiation rate k_1, as in equation (2). The value Ω in that equation may be considered as the frequency of the libration Γ_{4g} mode. This simple procedure allows us to reach full agreement with experimental data (curve a in figure 6).

With above values of $(I_{A'}/I_{A''})_{T=0}$, ΔE, k_2 and k_1 for $KZnF_3$:Tl^+ and taking into account the temperature dependence of k_1, we conclude that the luminescence intensity for temperatures $T \leqslant 100$ K is almost entirely due to the A″ transition, while at $T \geqslant 150$ K the luminescence is defined mainly by the A′ transition. Intensive luminescence in the whole temperature range results from the interplay of these two transitions.

Within the framework of the above fairly self-consistent pattern of optical phenomena in $KZnF_3$:Tl^+, the place of the second, weak A_1 luminescence band ($E_{max} = 4.66$ eV at 100 K) remains uncertain. At first sight it resembles a very weak luminescence at 5.1 eV (the A′ band position being at 5.8 eV), observed under A excitation at 20 K in $KMgF_3$:Tl^+ [6]. The authors of [6] connected this weak luminescence with internal processes of the excitation decay in the crystal matrix or with some alien admixtures, occasionally brought into samples. We are disposed to suppose, as was mentioned earlier, that at least in the case of $KZnF_3$:Tl^+ the A_1

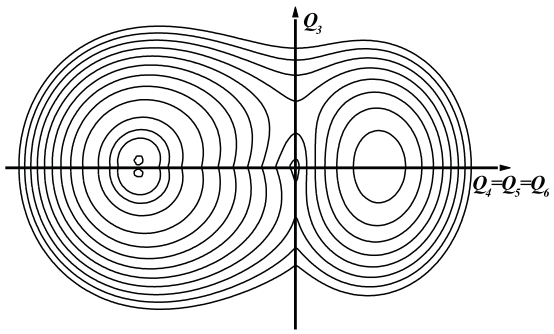

Figure 14. Contours of the lower sheet of APES of the $E(^3\Gamma^*_{4u}, Q)$-level in the plane containing trigonal and tetragonal distortions of the optical centre.

band is also due to the impurity Tl^+ ions. Indirect evidence for this is the similarity of excitation spectra of A′ and A_1 luminescence bands and the similarity of their decay kinetics (figures 3 and 6).

The presence of two luminescence bands (A_T and A_X) in alkali halide crystals is usually explained by the coexistence of two types of minimum on the lower APES sheets [7, 8]. However we did not observe the temperature dependence of the relative intensity of bands characteristic for such situations. Moreover, the position of the second A_1 band (4.66 eV) requires a second minimum, much deeper than the 'trigonal' minimum in figures 11 and 13, i.e., another set of parameters than that given in (27). Consequently we suppose that the A_1 band is, most likely, due to the defect centres with non-cubic positions of a Tl^+ ion. The band cannot be assigned to the dimer $(Tl^+)_2$ centres discussed, e.g., in [22], since, as mentioned in the experimental part, there is no regular dependence of the A_1 band intensity on the thallium concentration. The smaller value of A_1 luminescence lifetime agrees with the assumption that A_1 luminescence is due to the low symmetry defect Tl^+ centres. To clarify this and some other questions, further experimental (particularly polarization) measurements and theoretical investigations are necessary.

In connection with the problem of coexistence of different minima of adiabatic potential energies we give in figure 14 contours of the lower sheet of APES for the $^3\Gamma^*_{4u}$ level in the plane containing the trigonal axis ($Q_4 = Q_5 = Q_6$) and the tetragonal axis Q_3, near which the minima are situated when trigonal and tetragonal distortions are considered separately. One can see in figure 14 that the tetragonal minimum becomes a saddle point after taking into account trigonal deformations, while 'trigonal' minima undergo small changes (of position and depth) due to tetragonal distortions. Moreover, the search for global minima of APES in the six-dimensional space leads to a result close to the above trigonal minima, confirming the argumentation of the chosen model.

Now we shall discuss results of studying the $KMgF_3:Tl^+$ crystal. As mentioned before, at low temperatures the luminescence spectrum in this system differs substantially from that obtained in [6] by the intensive narrow peak (ZPL). This line is essentially very similar to that found in $KZnF_3:Tl^+$, and evidently has the same character in both systems: it is produced by the transition $^3\Gamma_{1u} \rightarrow {}^1\Gamma_{1g}$, allowed due to the hyperfine interaction and phonon-assisted mechanisms. The value $\tau_s^{-1} = 67\ s^{-1}$ at low temperatures is close to the radiation rate $k_1 = \tau_s^{-1} = 86\ s^{-1}$ in $KZnF_3:Tl^+$. The data on temperature dependence of τ_s^{-1} lead to the radiation rate $k_2 = 10^8\ s^{-1}$ for RES $^3\Gamma^*_{4u}$, also rather close to the value of k_2 in $KZnF_3:Tl^+$.

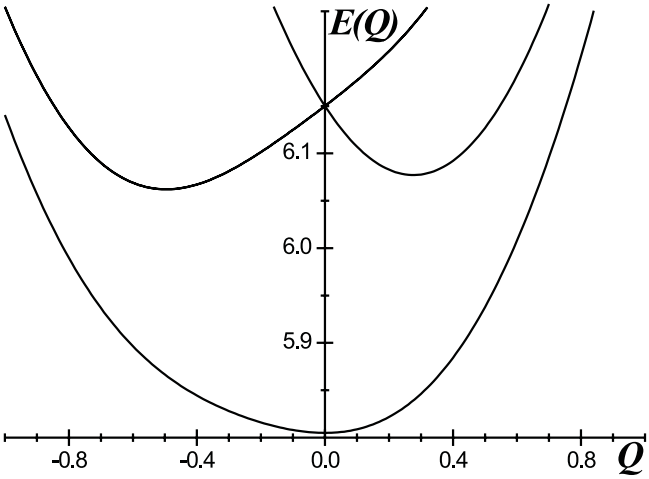

Figure 15. Cross-section of the APES $E(^3\Gamma_{1u})$, $E(^3\Gamma^*_{4u})$ for $KMgF_3$:Tl^+ by the plane, containing a trigonal axis.

However, the ratio $I_{A'}/I_{A''} = 2.57$ at 6 K in $KMgF_3$:Tl^+ is much larger than that in $KZnF_3$:Tl^+ (0.02), which, according to equation (12), leads to an essentially smaller coefficient of the nonradiative transition $k_{21}(0) = K = 4 \times 10^7\ s^{-1}$. Such a noticeable, by two orders of magnitude, reduction of the value K fully conforms with a larger value of $\Delta E = 207$ meV, compared to 147 meV for $KZnF_3$:Tl^+, following from the kinetics data (table 1). Provided that the nonradiative transition $2 \rightarrow 1$ proceeds with production of crystal lattice phonons having approximately Debye frequencies, the transition in the $KMgF_3$:Tl^+ system in comparison with $KZnF_3$:Tl^+ is accompanied by one or two extra phonons, the process takes place in the higher order of the perturbation theory over electron–vibration interaction and its probability essentially decreases. The similar spread of nonradiative transitions with the change of ΔE takes place also in other systems. Many data on such transitions in rare-earth compounds are systematized in the review [23].

The ratio $I_{A'}/I_{A''} = 2.57$ is essentially larger than the ratio of the fast and slow components (0.32 at 82 K) obtained in [6], probably due to different methods of resolving the fast and the slow components of luminescence.

The A' luminescence intensity in $KMgF_3$:Tl^+ is larger than that of A'' luminescence in the whole temperature range due to the above relation $k_2 \gg K$. However, due to the higher value of ΔE a fraction of A'' luminescence is noticeable even at temperatures of about 200 K: $I_{A'}/I_{A''}$ (200 K) ≈ 8, while for $KZnF_3$:Tl^+ at these temperatures $I_{A'}/I_{A''}$ (200 K) ≈ 37.

We have also calculated adiabatic potential energies for $KMgF_3$:Tl^+ in the space of trigonal displacements with the following parameter values, close to those used to fit the absorption band [1]:

$$\begin{aligned} &a^2 = a'^2 = 0.023, \qquad b^2 = 0.81, \qquad b'^2 = 0.49, \\ &c^2 = 1.8, \qquad c'^2 = 1,21, \qquad a_1 = a_2 = a_3 = 1.1, \\ &E_1(^3\Gamma_{1u}) = 5.805\ \text{eV}, \qquad E_A = 6.15\ \text{eV}, \\ &E_B = 7.38\ \text{eV}, \qquad E_C = 8.14\ \text{eV}. \end{aligned} \tag{31}$$

The cross-section of the APES by the plane, containing a trigonal axis, is given in figure 15. The value $\Delta E = 253$ meV again agrees well with the experiment. With parameters (31), we obtain the value $E_{A'} = E_{RES}(^3\Gamma^*_{4u}) - Q^2 = 5.83$ eV, corresponding to the experimental

position of the A′ band. Under comparatively small changes of parameters of the electron–phonon interaction, the value $E_{A'}$ can become both larger and smaller than the energy of the zero-phonon transition.

Though the A″ luminescence intensity in $KMgF_3:Tl^+$ is considerably less than the A′ luminescence intensity, the ZPL is observable up to temperatures of about 100 K, that is higher than in $KZnF_3:Tl^+$ (see figures 5 and 9). This may be explained by the form of the APES for the $^3\Gamma_{1u}$ state (compare figures 13 and 15): its minimum for $KMgF_3:Tl^+$ is pronounced much more strongly which leads to a weaker dependence of ZPL width on temperature.

It is seen that our experimental results satisfactorily fit the conventional theory of optical properties of systems containing ns^2 ions, if one uses appropriate sets of model parameters.

6. Summary

Our investigations (see [1, 2] and the present work) of the optical spectra of the fluoroperovskites $KZnF_3:Tl^+$ and $KMgF_3:Tl^+$ in the transition energy range of 1.5–6.4 eV at temperatures 4.2–300 K can be summarized as follows.

(i) An absorption band, A, with the temperature-dependent structure is observed in the indicated energy interval for both systems. The A band in $KZnF_3:Tl^+$ compared to that in $KMgF_3:Tl^+$ is shifted to lower energies by about 0.1 eV. A similar shift is observed for luminescence spectra of these systems. The position of the absorption bands in fluoroperovskites differs from that for a free thallium ion noticeably less than in alkali-halide crystals.

(ii) The luminescence patterns in two studied systems differ more appreciably. In both systems at low temperatures ($\leqslant$65 K) a narrow ZPL accompanied by vibration structure is observed. As the temperature increases, this line rapidly broadens and its intensity decreases. In both systems the broad intensive A′ band is observed at room temperature. As the temperature decreases, its intensity in $KZnF_3:Tl^+$ strongly diminishes and A″ luminescence becomes predominant at T about 100 K. In $KMgF_3:Tl^+$ the A′ intensity remains rather large and the vibration structure of the band becomes obvious. We note that the authors of [6] did not observe the zero-phonon line and the vibration structure of the A′ band in $KMgF_3:Tl^+$.

(iii) The studied optical centres refer to ns^2 ions in a cubic surrounding. Therefore a theory, developed by many authors and applied earlier mainly to alkali halide crystals, is used to analyse their properties. If the model parameters, defining the energy levels of s^2 and sp configurations of a two-electron system in cubic surroundings and the value of electron–vibration interaction, are properly chosen, the position and width of absorption and luminescence bands, the structure of bands and its dependence on temperature and also some kinetic characteristics can be satisfactorily described.

Acknowledgments

The work was partially supported by the Russian Foundation for Basic Research (project 02-98-18037) and by the Research and Educational Centre of Kazan State University (REC-007).

The authors are grateful to Professor B Z Malkin for useful discussions and Dr L V Mosina for help in the preparation of the manuscript.

References

[1] Aminov L K, Kosach A V, Nikitin S I, Silkin N I and Yusupov R V 2001 *J. Phys.: Condens. Matter* **13** 6247
[2] Aminov L K, Nikitin S I, Silkin N I and Yusupov R V 2002 *Phys. Solid State* **44** 1558

[3] Furetta C, Bacci C, Rispoli B, Sanipoli C and Scacco A 1990 *Radiat. Prot. Dosim.* **33** 107
[4] Scacco A, Fioravanti S, Missori M, Grassano U M, Luci A, Palummo M, Giovenale E and Zema N 1993 *Phys. Chem. Solids* **54** 1035
[5] Tsuboi T and Scacco A 1995 *J. Phys.: Condens. Matter* **7** 9321
[6] Scacco A, Fioravanti S, Grassano U M, Zema N, Nikl M, Mihokova E and Hamplova V 1994 *Phys. Chem. Solids* **55** 1
[7] Ranfagni A, Mugnai P, Bacci M, Viliani G and Fontana M P 1983 *Adv. Phys.* **32** 823
[8] Jacobs P W M 1991 *J. Phys. Chem. Solids* **52** 35
[9] Lakowicz J R 1983 *Principles of Fluorescence Spectroscopy* (New York: Plenum)
[10] Kazakov B N, Safiullin G M and Solovarov N K 1995 *Opt. Spectrosk.* **79** 426 (in Russian)
[11] Hlinka J, Mihokova E and Nikl M 1991 *Phys. Status Solidi* b **166** 503
[12] Seitz F 1938 *J. Chem. Phys.* **6** 150
[13] Van Vleck J H 1939 *J. Chem. Phys.* **7** 72
[14] Toyozawa Y and Inoue M 1966 *J. Phys. Soc. Japan* **21** 1663
[15] Merle d'Aubigne and Dang Le Si 1979 *Phys. Rev. Lett.* **43** 1023
[16] Ellervee A F, Laisaar A I and Oper A-M A 1981 *Pis. Zh. Eksp. Fiz.* **33** 24
[17] Abragam A and Bleaney B 1970 *Electron Paramagnetic Resonance of Transition Ions* (Oxford: Clarendon)
[18] Asano S 1981 *Phys. Status Solidi* b **105** 613
[19] Aminov L K 1978 *Spektroskopiya Kristallov* (Leningrad: Nauka) p 116
[20] Aminov L K, Kurkin I N, Silkin N I and Shlenkin V I 1975 *Phys. Status Solidi* b **72** 97
[21] Rebane K K 1968 *Elementarnaya Teoriya Kolebatel'noi Struktury Spektrov Primesnykh Tsentrov Kristallov* (Moskva: Nauka)
[22] Tsuboi T and Jacobs P W M 1991 *J. Phys. Chem. Solids* **52** 69
[23] Malkin B Z 2003 *Spectroscopic Properties of Rare Earths in Optical Materials* ed G K Liu and B Jacquier (Berlin: Springer) at press